International Journal of Solids and Structures 47 (2010) 1449–1458

Contents lists available at ScienceDirect

International Journal of Solids and Structures

journal homepage: www.elsevier.com/locate/ijsolstr

Multiparameter actuation for shape control of bistable composite plates

Amâncio Fernandes [a,b], Corrado Maurini [a,b,*], Stefano Vidoli [c]

[a] UPMC Univ. Paris 06, UMR 7190, Institut Jean Le Rond d'Alembert, F-75005 Paris, France
[b] CNRS, UMR 7190, Institut Jean Le Rond d'Alembert, F-75005 Paris, France
[c] Univ. Roma La Sapienza, Dip. Ingegneria Strutturale e Geotecnica, via Eudossiana 18, 00184, Rome, Italy

ARTICLE INFO

Article history:
Received 31 August 2009
Received in revised form 9 February 2010
Available online 18 February 2010

Keywords:
Morphing structures
Stability
Nonlinear plate theory
Gaussian curvature
Shape control

ABSTRACT

This paper studies the stable equilibrium shapes of free multilayered orthotropic plates loaded by inelastic deformations induced by thermal and piezoelectric effects. Starting with a Von Kármán plate kinematics and an energetic formulation, a discrete intrinsic nonlinear model in terms of curvatures only is deduced. The model has 3 degrees of freedom, namely the components of the symmetric curvature tensor, which is supposed to be uniform in space. Despite of this rough assumption, the analytical results about the equilibrium shapes and their stability show a good agreement with the finite element simulations performed with a commercial code. Literature results about the bistable behavior of isotropic plates under a single-parameter loading are extended to the orthotropic case with two loading parameters. In light of a global stability analysis and a phase portrait as a function of the inelastic curvatures, we study possible actuation techniques for controlling the transition of the plate between its two stable configurations. We show that with a suitable two-parameter actuation, it is possible to get a controlled quasi-static transition, avoiding any instability phenomenon. Numerical simulations on a realistic case study support the technological feasibility of the proposed actuation technique when using active piezoelectric layers to control the inelastic curvature.

1. Introduction

In slender structures geometrical effects may induce complex non-linear phenomena. Beams, arches, plates, and shells may exhibit several stable equilibrium configurations very different in shape. The passage from one configuration to another may take place with small deformations and with an approximately linear elastic material behavior. These properties attract the interests of the engineering community to conceive multistable structures able to hold without an external actuation several equilibrium shapes, each one associated to a specific functional regime. Hence, active materials with limited actuation power may be efficiently employed to induce great changes in shape by triggering the passage between several stable equilibria.

The design of morphing multistable structures with embedded actuation is a challenging problem from the theoretical and technologic point of view. It demands to face two main difficulties: (i) taking into account non-linear effects to design a structure with a set of assigned stable equilibrium configurations; (ii) conceiving efficient actuation techniques to control the transition among different equilibria. The starting point to tackle these issues is a careful study and a synoptic representation of the non-linear static behavior of the considered class of structures. This may be obtained only on the basis of simplified low-dimensional models, resuming the foremost qualitative properties of the system. Finite element numerical studies may constitute a validation tool in a second step of the analysis, keeping in mind that the numerical analysis of non-linear systems with multiple stable equilibria remains a difficult task.

Thin structures as plates and shells appear as good candidates for shape-changing applications. In plate and shells, multistability is a consequence of the geometrical coupling between the Gaussian curvature and the membrane distortions. Previous works show that shallow orthotropic shells may exhibit up to three stable configurations with almost uniform curvature, depending on their initial shape and material parameters (Guest and Pellegrino, 2006; Seffen, 2007; Vidoli and Maurini, 2008). In corrugated shells, local and global deformation modes may be coupled together to provide a rich multistable behavior (Norman et al., 2008, 2009). In multilayered plates assembled in a flat mold, the mismatch of the inelastic strains at different layers may induce residual stresses responsible for bifurcation phenomena and multiple stable equilibrium positions. The differential inelastic strains may be associated to thermal or hygroscopic loads, electromechanical couplings in active materials, growth, or plasticity. Similar effects are well documented, being encountered in various applicative contexts, including unsymmetric composite laminates (Hyer, 1981a,b; Potter et al., 2007; Mattioni et al., 2007), thin-film/substrate systems extensively used in microelectronic applications, MEMS, thermal barrier coatings, thin-film coatings (Finot and Suresh, 1996; Freund, 2000; Dunn et al., 2002;

* Corresponding author. Tel.: +33 1 44 27 87 19; fax: +33 1 44 27 52 59.
E-mail address: corrado.maurini@upmc.fr (C. Maurini).

0020-7683/$ - see front matter © 2010 Elsevier Ltd. All rights reserved.
doi:10.1016/j.ijsolstr.2010.02.007

Zhang and Dunn, 2004), biological systems (Forterre et al., 2005; Dervaux and Ben Amar, 2008).

The present work focuses on the multistability of multilayered plates and its potential application to shape control of composite panels by active materials. It is organized in three main parts. In the first part, including Sections 2 and 3, we derive a simple analytical model for a free orthotropic Föppl–Von Kármán plate with inelastic deformations. This is an intrinsic model (Ciarlet et al., 2009) which uses the curvature as main kinematical descriptor (Guest and Pellegrino, 2006; Seffen, 2007; Seffen and McMahon, 2007). The model is based on the key simplifying hypothesis of considering states with uniform curvature. It allows us to illustrate the global picture of the nonlinear behavior on the basis of analytical results. Specifically, we discuss the number and shape of stable equilibria as functions of the control parameters, representing the inelastic curvatures applied in two orthogonal directions. In this respect, we generalize to the generic orthotropic case and to multiparameter loadings the analytical results reported in Salamon and Master (1995), Finot and Suresh (1996), Freund (2000), and Seffen and McMahon (2007), giving a concise interpretation of the numerical results of Hyer (1981a), Hyer (1981b), Dano and Hyer (2002), and Gigliotti et al. (2004).

In the second part (Section 4), we revisit the phenomena of bistability of unsymmetric laminates in light of a global phase portrait as a function of the inelastic curvatures. Hence, we discuss qualitatively the possible actuation modes for controlling the transition between two stable shapes through embedded active layers. Namely, besides the well-documented snap-through phenomenon, which can be induced with a single parameter actuation (Mattioni et al., 2007; Portela et al., 2008), we show that, by using two independent actuating parameters, it is possible to let the plate pass from one stable configuration to the other in a purely quasi-static fashion, following a path of stable equilibria. This extends to the case of plates a similar idea proposed in Maurini et al. (2007) for buckled beams.

The third part of the paper (Section 5) presents an applicative example of the proposed two-parameter actuation technique for a laminate plate including active layers of piezoelectric fiber composites. The aim here is two-fold: (i) to assess the technical feasibility of the proposed concepts, giving the typical order of magnitude of the values of the physical parameters and the technologic constraints, especially on the available actuation forces; (ii) to validate the results of the analytical model by fully nonlinear simulations obtained with a commercial finite element code.

2. Uniform curvature Föppl–Von Kármán model of composite plates

2.1. Kinematics

Consider a plate $\mathscr{S}$ and let us label its material points by their cartesian coordinates (x,y) in a flat configuration. Let $u=(u_x,u_y)$ and w denote, respectively, the in-plane and transverse displacement fields. In unshearable plate models, the deformations are represented by two 2×2 symmetric tensor fields, the in-plane distortion $e=(e_x,e_y,2e_{xy})^T$ and the curvature $k=(k_x,k_y,2k_{xy})^T$; here and henceforth their independent components are listed in columns by using the standard Voigt notation. According to the Von Kármán kinematics, the compatibility relations between deformations and displacements read as (see e.g. Mansfield, 1989):

$$\begin{aligned} &e_x(u,w)=\frac{\partial u_x}{\partial x}+\frac{1}{2}\left(\frac{\partial w}{\partial x}\right)^2,\quad e_y(u,w)=\frac{\partial u_y}{\partial y}+\frac{1}{2}\left(\frac{\partial w}{\partial y}\right)^2,\\ &e_{xy}(u,w)=\frac{1}{2}\left(\frac{\partial u_x}{\partial y}+\frac{\partial u_y}{\partial x}\right)+\frac{1}{2}\left(\frac{\partial w}{\partial x}\frac{\partial w}{\partial y}\right),\\ &k_x(w)=\frac{\partial^2 w}{\partial x^2},\quad k_y(w)=\frac{\partial^2 w}{\partial y^2},\quad k_{xy}(w)=\frac{\partial^2 w}{\partial x\partial y}. \end{aligned} \tag{1}$$

The in-plane distortion includes the second-order geometric contributions due to transverse displacements. They are the source of the nonlinear behavior.

Eq. (1) imply the following compatibility condition between the in-plane distortion e and the curvature k:

$$\mathscr{L}(e):=\frac{\partial^2 e_y}{\partial x^2}+\frac{\partial^2 e_x}{\partial y^2}-2\frac{\partial^2 e_{xy}}{\partial x\partial y}=\det k, \tag{2}$$

where $\det k=k_xk_y-k_{xy}^2$ is the Gaussian curvature of the plate current configuration and $\mathscr{L}$ is a linear second-order differential operator. Eq. (2) represents the linearized version of the Gauss Theorema Egregium around a flat configuration. If the deformation fields (e,k) do not verify the equation above, equations (1) are not integrable. This means that it is impossible to find a configuration of the plate with the given (e,k), without cutting the plate. The compatibility relation (2) is an extremely useful intrinsic statement of the coupling between in plane-extension and the Gaussian curvature. Especially, it shows that any change of Gaussian curvature implies a non-uniform in-plane distortion.

2.2. Constitutive behavior

The generalized stresses of the plate are represented by the 2×2 symmetric tensor fields $\sigma=(\sigma_x,\sigma_y,\sigma_{xy})^T$ and $m=(m_x,m_y,m_{xy})^T$. They are defined as the force and moment resultants of the contact actions across the plate thickness. Composite plates with linear material behavior are characterized by the following constitutive relations:

$$\sigma(e,k)=\overline{A}(e-e_R)+\overline{B}(k-k_R), \tag{3a}$$

$$m(e,k)=\overline{B}^T(e-e_R)+\overline{D}(k-k_R), \tag{3b}$$

where $\overline{A}$, $\overline{B}$, and $\overline{D}$ are the standard 3×3 matrices of composite plate theory, representing in the Voigt notation the extensional stiffness, the extension-to-bending coupling, and the bending stiffness, respectively (see e.g. Berthelot, 1999). Eq. (3) account for the fact that the flat configuration with $e=0$, $k=0$ may be not stress-free. The tensors $e_R=(e_{Rx},e_{Ry},2e_{Rxy})^T$ and $k_R=(k_{Rx},k_{Ry},2k_{Rxy})^T$ model inelastic deformations as those associated to thermal or plastic effects, material growth, or the presence of active materials, as piezoelectrics. They may be interpreted as deformations in a *relaxed* (stress-free) *stance*. We borrow the term *relaxed stance* from DiCarlo and Quiligotti (2002) to underline that the configuration with zero-stress may be geometrically unreachable, because e_R and k_R need not to satisfy the implicit compatibility condition (2). Our analysis will be restricted to the case where k_R is constant in space. We allow for non-constant in-plane inelastic deformations e_R, but we do assume that $\mathscr{L}(e_R)$ is constant.

For the following developments is useful to define the bending stiffness at null membrane stress ($\sigma=0$), namely $\widetilde{D}=\overline{D}-\overline{B}^T\overline{A}^{-1}\overline{B}$. We further introduce its non-dimensional version as $D:=\widetilde{D}/\widetilde{D}_{11}$. For orthotropic plates, D may be written in the form

$$D=\begin{bmatrix}1 & \nu & 0\\ \nu & \beta & 0\\ 0 & 0 & \rho(1-\nu^2/\beta)\end{bmatrix}, \tag{4}$$

where $\beta=\widetilde{D}_{22}/\widetilde{D}_{11}$, $\nu=\widetilde{D}_{12}/\widetilde{D}_{11}$, $\rho=\widetilde{D}_{33}\widetilde{D}_{22}/(\widetilde{D}_{11}\widetilde{D}_{22}-\widetilde{D}_{12}^2)$.

2.3. Potential energy

We look for the shapes of the stable equilibria as functions of the inelastic deformations e_R and k_R, which we regard as control parameters. For plates without applied forces, the total potential energy reads as

$$\mathscr{U}(u,w) = \frac{1}{2}\int_{\mathscr{S}} \overline{A}(e(u,w)-e_R)\cdot(e(u,w)-e_R)d\overline{S} + \int_{\mathscr{S}} \overline{B}^T(e(u,w)-e_R)\cdot(k(w)-k_R)d\overline{S} + \frac{1}{2}\int_{\mathscr{S}} \overline{D}(k(w)-k_R)\cdot(k(w)-k_R)d\overline{S}, \quad (5)$$

where e and k are given by (1) and $d\overline{S}$ is the surface element. The first term of (5) is the membrane energy, the third term is the bending energy, and the second term is due to the bending-to-membrane constitutive coupling. The stable equilibria are then defined as the local minimizers of (5) in the spaces of admissible in-plane and transverse displacements u and w.

2.4. Uniform curvature hypothesis

Focusing on plates free at the boundaries, without applied forces, and with uniform inelastic curvatures k_R, we look for approximate analytical solutions by introducing the key hypothesis that the curvature k is constant throughout the plate, i.e. that

$$w = w_k(x,y) := \frac{1}{2}k_x x^2 + \frac{1}{2}k_y y^2 + k_{xy}xy \quad (6)$$

with constant k_x, k_y, and k_{xy}. By using the uniform curvature hypothesis, the potential energy may be rewritten as

$$\widetilde{\mathscr{U}}(u,k) = \frac{1}{2}\overline{S}\widetilde{D}(k-k_R)\cdot(k-k_R) + \frac{1}{2}\int_{\mathscr{S}} \overline{A}^{-1}\sigma\cdot\sigma d\overline{S}, \quad (7)$$

where $\widetilde{D}$ is the bending stiffness at $\sigma = 0$ defined in Section 2.2, $\overline{S}$ is the surface of the plate, and[1]

$$\sigma = \overline{A}(e(u,w_k)-e_R) + \overline{B}(k-k_R). \quad (8)$$

The stable equilibria are now the minima of (7) and (8) with respect to u and k. Yet, one can solve the membrane problem to obtain an intrinsic discrete model in terms of curvature only.

2.5. Membrane problem

The stationarity condition of (7) with respect to u gives the equilibrium equations for the in-plane problem, which read as

$$\operatorname{div}\sigma = 0 \quad \text{on } \mathscr{S} \qquad \text{and} \qquad \sigma n = 0 \quad \text{on } \partial\mathscr{S}, \quad (9)$$

where n is the normal to the boundary $\partial\mathscr{S}$, supposed to be free. Eq. (9) together with the constitutive equations (8) and the compatibility conditions (1) constitute a *linear* problem of plane elasticity, which may be solved univocally as a function of k. For the present case of a free plate in which there are not boundary conditions on the displacement field, the membrane problem may be conveniently reformulated in terms of stresses, by using the implicit compatibility equation (2). For an homogeneous plate with uniform $\overline{A}$, $\overline{B}$, k and k_R, solving (8) with respect to e, substituting into (2), and accounting for the linearity of $\mathscr{L}$ gives:

$$\mathscr{L}(\overline{A}^{-1}\sigma) = \det k - \mathscr{L}(e_R). \quad (10)$$

The right-hand side of Eq. (10) is the mismatch between the actual Gaussian curvature and the Gaussian curvature associated to the in-plane inelastic deformations e_R. If $\mathscr{L}(e_R) = 0$, as obtained for uniform inelastic deformations, the only forcing term in the linear system of Eqs. (9) and (10) is the Gaussian curvature $\det k$ and the solution for σ must be in the form

$$\sigma = \overline{A}_{11}L^2\Sigma(x,y)\det k, \quad (11)$$

where $L := \sqrt{\overline{S}}$ is the typical in-plane dimension of the plate and $\Sigma(x,y)$ is a non-dimensional tensor function giving the stress distribution.

Remark 2.1. The function $\Sigma(x,y)$ may be determined solving the boundary value problem (9) and (10) for $\det k = 1/(\overline{A}_{11}L^2)$. Numerically, this task may be accomplished using a standard finite element code for plane elasticity (in plane-stress condition) with inelastic strain. Indeed, on the basis of Eq. (10), the membrane stresses generated by a non-null uniform gaussian curvature are equivalent to those induced by inelastic strains e_R with $\mathscr{L}(e_R) = -\det k$. For example, one may obtain the function $\Sigma(x,y)$ through the solution of the plane stress elasticity problem with $e_{Rx} = -y^2/(2\overline{A}_{11}L^2)$, $e_{Ry} = e_{Rxy} = 0$.

2.6. Intrinsic model in terms of curvatures only

Substituting the solution (11) for the membrane problem into (7) gives an expression for the energy in terms of the curvature only. Here, we define the non-dimensional actual and inelastic curvatures $K = \{K_x, K_y, 2K_{xy}\}$ and $H = \{H_x, H_y, 2H_{xy}\}$ by adopting the scaling

$$(K_x, H_x) = R_0(k_x, k_{Rx}), \quad (12a)$$

$$(K_y, H_y) = R_0\sqrt{\beta}(k_y, k_{Ry}), \quad (12b)$$

$$(K_{xy}, H_{xy}) = R_0\sqrt[4]{\beta}(k_{xy}, k_{Rxy}), \quad (12c)$$

and choosing the scaling radius of curvature as

$$R_0 := \psi L^2\sqrt{\frac{\overline{A}_{11}}{\widetilde{D}_{11}}} \quad \text{with } \psi := \sqrt{\int_{\mathscr{S}} A^{-1}\Sigma\cdot\Sigma dS}, \quad (13)$$

where $dS := d\overline{S}/L^2$ and $A := \overline{A}/\overline{A}_{11}$ are the non-dimensional element of area and membrane stiffness. With this special scaling, the non-dimensional version of the energy function (7) can be simplified to get

$$U(K) = \frac{1}{2}D^*(K-H)\cdot(K-H) + \frac{1}{2}(\det K)^2, \quad (14)$$

where

$$D^* = \begin{bmatrix} 1 & \mu & 0 \\ \mu & 1 & 0 \\ 0 & 0 & \gamma \end{bmatrix} \quad (15)$$

is a bending stiffness matrix for a material with the same stiffness in the two principal directions. The equivalent Poisson ratio μ, and non-dimensional shear modulus γ are defined as

$$\mu = \frac{\nu}{\sqrt{\beta}}, \quad \gamma = \frac{\rho(1-\nu^2/\beta)^2}{\sqrt{\beta}}. \quad (16)$$

The stable equilibria of the plate under the uniform curvature hypothesis may be obtained by minimizing $U(K)$ for $K = (K_x, K_y, 2K_{xy})^T \in IR^3$. This problem is purely algebraic and may be tackled analytically.

2.7. Remarks

To conclude this section, we resume below some remarks on the presented uniform curvature model of orthotropic plates with inelastic deformations.

Remark 2.2. The interest of the "anisotropic" scaling (12) is to reduce the problem for a generic orthotropic plate, to the one for an equivalent square symmetric[2] composite. Especially, this clearly

[1] For the sake of brevity, the notation for σ omits the explicit dependence on u and w.

[2] In composite theory square symmetric materials are characterized by having the same stiffness in the two principal directions (Love, 1906).

shows that there are only two relevant material parameters affecting the uniform-curvature solutions of orthotropic Föppl–Von Kármán plates: μ and γ. A change of β, the ratio between the Young moduli in the two coordinate directions, is tantamount to a rescaling of the curvatures.

Remark 2.3. The shape of the plate planform $\mathscr{S}$ enters in the uniform curvature model (14) only through the definition of the scaling factor ψ for the characteristic radius R_0 in Eq. (13). This is a direct consequence of the uniform curvature hypothesis and in contrast with the results of more accurate models. For example, finite element numerical simulations on rectangular plates show that the aspect ratio between the edge lengths influences the system behavior in nonlinear regimes (Freund, 2000; Gigliotti et al., 2004). The uniform curvature model is not able to predict this effect.

Remark 2.4. Seffen (2007), Vidoli and Maurini (2008) studied, with the same uniform curvature hypothesis, the multistability of orthotropic shallow shells as a function of their initial curvature in a stress free configuration. Up to a suitable scaling of the curvatures, the associated energy function is

$$U(K) = \frac{1}{2} D^*(K-H)\cdot(K-H) + \frac{1}{2}(\det K - \det H)^2. \tag{17}$$

This case can be recovered from the present model by considering compatible inelastic deformations (e_R, k_R) with non-vanishing Gaussian curvature such that $\mathscr{L}(e_R) = \det k_R \neq 0$.

Remark 2.5. The presence of the constitutive coupling between membrane distortion and bending, controlled by the matrix B, affects only the coefficient of the equivalent bending stiffness without altering the structure of the energy function and the qualitative properties of the solutions. Also, adding uniform membrane inelastic deformations (e_R with $\mathscr{L}(e_R) = 0$) is immaterial in the present model.

3. Equilibria and stability

We study how the equilibria of the plate and their stability properties depend on the inelastic curvatures H_x and H_y, supposing $H_{xy} = 0$. In the proposed uniform curvature model, the equilibria are the points of stationarity of (14), i.e. the solutions of

$$K_x - H_x + \mu(K_y - H_y) + K_y \det K = 0, \tag{18a}$$
$$K_y - H_y + \mu(K_x - H_x) + K_x \det K = 0, \tag{18b}$$
$$2K_{xy}(\det K - 2\gamma) = 0, \tag{18c}$$

where the Gaussian curvature $\det K = K_x K_y - K_{xy}^2$ is the source of nonlinearity in the system behavior. The stability of an equilibrium position K depends on the sign of the Hessian matrix

$$\frac{\partial^2 U}{\partial K^2} = \begin{pmatrix} K_y^2+1 & 2K_xK_y+\mu-K_{xy}^2 & -2K_{xy}K_y \\ 2K_xK_y+\mu-K_{xy}^2 & K_x^2+1 & -2K_{xy}K_x \\ -2K_{xy}K_y & -2K_{xy}K_x & 6K_{xy}^2+4\gamma-2K_xK_y \end{pmatrix}. \tag{19}$$

When the matrix is positive definite the equilibrium is stable. Remarkably in the present case the stability depends only on the position in the state space $K_x - K_y$, the Hessian being independent of the control parameters H_x and H_y. As noted by Seffen and McMahon (2007), some properties of the solutions of the nonlinear system of Eq. (18) may be deduced by looking at the third equilibrium equation (18c), which implies that either $K_{xy} = 0$ or $\det K = 2\gamma$. In other words equilibria for $H_{xy} = 0$ may be untwisted or twisted, but the twisted ones are with assigned Gaussian curvature. The following discussion distinguishes the two cases.

3.1. Untwisted equilibria

The equilibrium equations for the untwisted equilibria, $K_{xy} = 0$, are nonlinear in K_x and K_y. Yet, their stability is rather simple to be studied. The Sylvester's criterion for the positive definiteness of the Hessian matrix (19) at $K_{xy} = 0$ implies that the untwisted equilibria are stable if the following two conditions are satisfied:

$$(1+K_y^2)(1+K_x^2) - (2K_xK_y+\mu)^2 > 0, \tag{20a}$$
$$2\gamma - K_xK_y > 0. \tag{20b}$$

In the special case of equal or opposite inelastic curvatures in the two coordinate directions, closed-form solutions for the untwisted equilibria are available. Namely, for $H_x = h$ and $H_y = \pm h$, we find three solutions of the equilibrium equations, say $K^{(1)}$, $K^{(2)}$, and $K^{(3)}$, given by

$$K_x^{(1)} = \pm K_y^{(1)} = \frac{\sqrt[3]{2}\sqrt[3]{f^2(h,\pm\mu)} - 2\sqrt[3]{3}(1\pm\mu)}{6^{2/3}\sqrt[3]{f(h,\pm\mu)}}, \tag{21a}$$

$$K_x^{(2)} = \pm K_y^{(3)} = \frac{h}{2}(1\pm\mu) + \sqrt{\frac{h^2}{4}(1\pm\mu)^2 - (1\mp\mu)}, \tag{21b}$$

$$K_x^{(3)} = \pm K_y^{(2)} = \frac{h}{2}(1\pm\mu) - \sqrt{\frac{h^2}{4}(1\pm\mu)^2 - (1\mp\mu)}, \tag{21c}$$

where the upper sign is for $H_x = H_y = h$, the lower sign for $H_x = -H_y = h$, with

$$f(h,\mu) = (1+\mu)\left(\sqrt{3}\sqrt{27h^2 + 4(1+\mu)} + 9h\right).$$

The first equilibrium $K^{(1)}$ is always real. The second and third equilibrium, $K^{(2)}$ and $K^{(3)}$, are real for $|h| \geqslant h_P^{\pm}$, with

$$h_P^{\pm} = 2\frac{\sqrt{1\mp\mu}}{1\pm\mu}. \tag{22}$$

For $h = h_P^{\pm}$ the three equilibria coalesce at the critical points $K_x = \pm K_y = \pm k_P$ with $k_P = \sqrt{1+\mu}$. These two critical points are cusp catastrophes for the energy function (7), associated to pitchfork bifurcations in the $K_x - K_y$ plane at $K_{xy} = 0$.

3.2. Twisted equilibria

The solution for the twisted equilibria ($K_{xy} \neq 0$) is simple because they have assigned Gaussian curvature $\det K = 2\gamma$. Using this property, the equilibrium equations become linear in K_x and K_y and may be solved to get

$$K_x = \frac{H_x(1-\mu(\mu+2\gamma)) - 2\gamma H_y}{1-(\mu+2\gamma)^2}, \tag{23a}$$

$$K_y = \frac{H_y(1-\mu(\mu+2\gamma)) - 2\gamma H_x}{1-(\mu+2\gamma)^2}, \tag{23b}$$

$$K_{xy} = \pm\sqrt{K_xK_y - 2\gamma}. \tag{23c}$$

These equilibria are real only if $K_xK_y \geqslant 2\gamma \geqslant 0$. In particular, plates with negative Gaussian curvature admit only untwisted equilibria if $H_{xy} = 0$. For $H_x = H_y = h$, twisted equilibria become possible for

$$|h| > h_Q = \sqrt{2\gamma}\frac{1+2\gamma+\mu}{1+\mu}. \tag{24}$$

At $|h| = h_Q$ the energy function (7) presents a cusp catastrophe, associated to a pitchfork bifurcation along the K_{xy}-axis at the point $K_x = K_y = k_Q, K_{xy} = 0$, with $k_Q = \sqrt{2\gamma}$.

3.3. Conclusion and stability diagrams

Figs. 1 and 2 illustrate the behavior of the system for $\mu = 0.156$, $\gamma = 0.184$. These values of the non-dimensional parameters correspond to the material data and geometry of the case study detailed in Section 5. Fig. 1 reports (a) the partition of the state space $K_x - K_y$ (untwisted equilibria) in stability regions according to the criteria (20) and (b) a phase portrait of the system as a function of the inelastic curvatures $H_x - H_y$. The latter diagram distinguishes among regions of bistability (gray) and monostability (white); the solid lines mark the inelastic curvatures for which at least one of the equilibria has an eigenvalue of the Hessian matrix (19) changing in sign, corresponding to the limit of stability of a specific curvature mode. Fig. 2 illustrates the curvatures of the stable equilibria when moving along the bisectors of Fig. 1(b). Looking at these diagrams in light of the analytical results of the previous subsections, we observe two distinct behaviors depending on the sign of the inelastic Gaussian curvature:

1. For inelastic deformations with *negative Gaussian curvature* ($H_xH_y < 0$), only *untwisted* equilibria are possible. The critical point P^- in Figs. 1 and 2(a) corresponds to a cusp catastrophe, with a pitchfork bifurcation at $K_{xy} = 0$. For inelastic curvatures in the bistability region (gray), as in point A of Fig. 1b, two stable equilibria are possible: one ($K^{(2)}$) with a large curvature in the x direction, the other ($K^{(3)}$) with a large curvature in the y direction. For $H_y = -H_x$ their analytical expressions are given in Eq. (21). Note that if the inelastic curvature H varies continuously from the point A, when crossing the limit of the bistability region, one of the equilibria disappears. The other varies continuously with H, keeping its stability. Especially, the surviving equilibrium is the one with large curvature in the y direction (resp. x direction) when crossing the arc $R - P^-$ (resp. $S - P^-$). These properties will be used extensively in the following.
2. For inelastic deformations with *positive Gaussian curvature* ($H_xH_y > 0$), *twisted* and *untwisted* equilibria are admissible. There are two possible modes of bifurcation when moving along the line $H_x = H_y = h$:
   (a) a pitchfork bifurcation at $K_{xy} = 0$ as in Eq. (21) for $h = h_P^+$, which is equivalent to the one observed for negative Gaussian curvatures (critical point P^+ in Fig. 1b), and
   (b) a pitchfork bifurcation where an untwisted equilibrium bifurcates in two stable twisted ones for $h = h_Q$ (critical point Q in Fig. 1b), according to Eq. (23).

Comparing the values of h_P^+ and h_Q of equations (22) and (24), we may conclude that the first phenomenon occurs for large values of the shear stiffness, namely for $\gamma > (1-\mu)/2$, while the second one is observed for $\gamma < (1-\mu)/2$. Figs. 1 and 2b refer to the latter case.

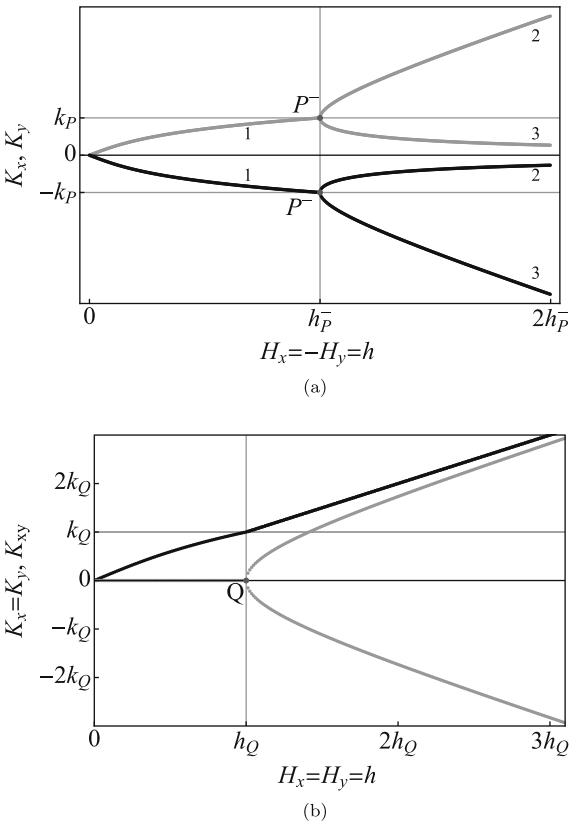

Fig. 2. Bifurcation diagrams as the inelastic curvature H is changed: (a) along the segment OA and (b) along the segment OP^+ in Fig. 1b. In (a) black and gray lines mark the K_x and K_y components respectively, being $K_{xy} = 0$; in (b) black is for $K_x = K_y$ whilst gray is for K_{xy}.

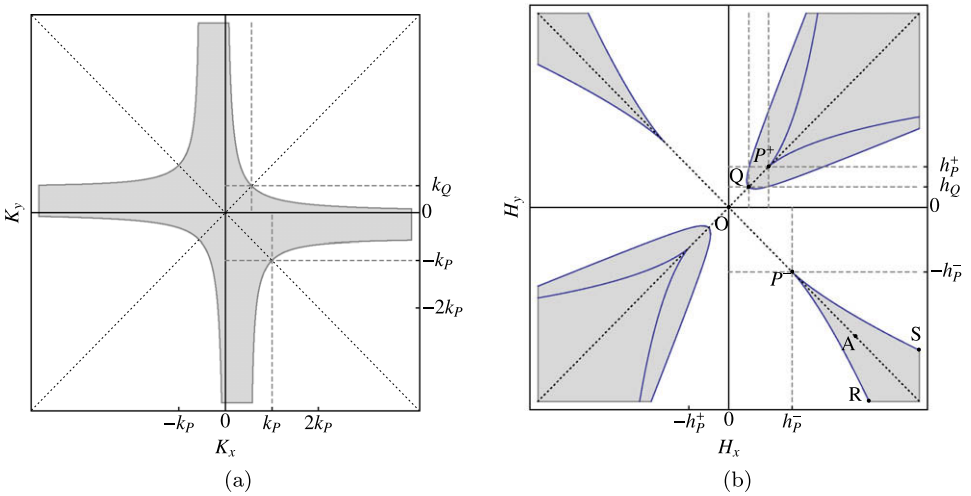

Fig. 1. Stability diagrams as functions of the actual and inelastic curvatures: in (a) the gray region corresponds to curvatures $K_x - K_y$ for which the stability criteria (20b) for untwisted configurations are satisfied; in (b) the white and gray regions, respectively, denote mono- and bi-stability with respect to $H_x - H_y$ parameters. All the possible stability boundaries are reported as thin solid lines.

Remark 3.1. The analysis above generalizes the literature results on the stability and bifurcation of plates with inelastic deformations. Previous works (e.g. Salamon and Master, 1995; Freund, 2000; Seffen and McMahon, 2007) provide analytical and numerical results only for the case of isotropic plates as a function of a single control parameter (e.g. the parameter h for the case $H_x = \pm H_y$). The present results give the qualitative system behavior for generic H_x and H_y and resume in a condensed form the analytical results for $H_x = \pm H_y$. We show also that this behavior and the associated analytical results are generic for orthotropic plates. All the analytical formulas may be transposed to the dimensional form by using equations (12).

Remark 3.2. For isotropic plates the shear stiffness is not a free parameter, being $\gamma = (1-\mu)^2(1+\mu)/2$. Especially, γ is always smaller than the critical value $(1-\mu)/2$ ruling the order between points Q and P^+. However, in the isotropic case the elastic energy is invariant for rotations and the twisting mode is energetically indifferent (i.e. all configurations differing by a twist are at the same energy level). This means that the cusp catastrophe with respect to twist at the point Q degenerates and no bifurcation with respect to twist appears. This may explain why the studies on isotropic plates (Salamon and Master, 1995; Freund, 2000; Seffen and McMahon, 2007) report only the pitchfork bifurcation in the $K_x - K_y$ plane at the point P^+.

4. Actuation of bistable plates

In this section we analyze possible actuation techniques of bistable plates using the results of the global stability analysis presented above. The aim is to determine how is possible to induce the passage between the two stable configurations of the plate by controlling the inelastic curvatures. These curvatures may be induced by various physical effects: thermal strains, plastic deformations, piezoelectric coupling, phase-transitions, growth.

To fix ideas, we consider the actuation through embedded active layers of bistable unsymmetric laminates. As discussed in several numerical and experimental works (Hyer, 1981a,b), unsymmetric laminates may be bistable because of the inelastic curvatures due to the thermal effects experienced during the curing process. The [0/90] cross-ply studied by Hyer is assembled at high temperature in a flat mold. At ambient temperature differential thermal strains in the two layers induce an inelastic curvature H_A equal and opposite in the x and y directions, as in the point A of Fig. 3(b). The plate is bistable with the two stable shapes corresponding to the points A_2 and A_3 in Fig. 3(a). Adding active layers (e.g. piezoelectric Macro Fiber Composites) makes possible to further control the inelastic curvatures H_x and H_y around H_A. In the following, after reviewing the phenomena that can be obtained with a single-parameter actuation, we show that a multiparametric actuation may open novel interesting scenarios.

4.1. Single-parameter actuation: snap-through

Several authors investigated the use of a piezoelectric actuator to control the transition between the two equilibria of the bistable plate (Schultz et al., 2006; Portela et al., 2008). The effect of a single actuator made of piezoelectric fiber composite is equivalent to an induced inelastic curvature applied along a specific direction, say H_y, which will add to the initial inelastic curvature H_A. Being controlled by the applied piezoelectric voltage, the total inelastic curvature moves from H_A along the line AE of Fig. 3(b). Correspondingly, if the system configuration is initially in the state A_3, the actual configuration of the plate moves along the curve A_3F_3 of Fig. 3(a). When the inelastic curvature reaches the boundary of the bistability region at point F, the current configuration becomes unstable; thus the plate snap-through towards the other possible equilibrium, F_2, which is still stable. When resetting to zero the piezoelectric actuation, the inelastic curvature comes back to H_A, but the plate holds now the equilibrium position A_2 (see also the Supplementary Material S2). This kind of passage between the configurations $A_3 \to A_2$ happens dynamically, with a snap-through phenomenon. Note that the inverse passage $A_2 \to A_3$ with the same actuation mode requires to exit from the bistability region at the point R. This demands a higher actuation voltage because the segment AR is longer than the segment AF.

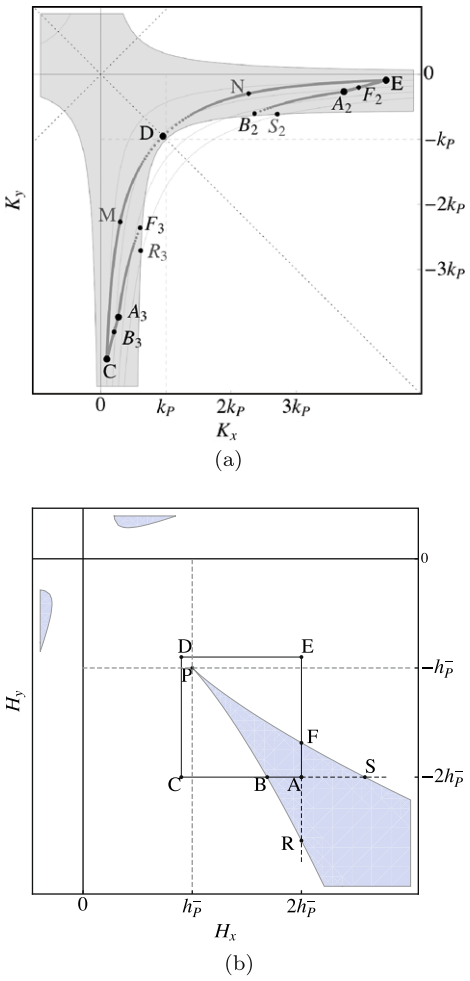

Fig. 3. Stability diagrams illustrating stable transition paths between the stable equilibria A_3 and A_2. As in Fig. 1, (a) reports a stability diagram in the $K_x - K_y$ plane, whilst (b) reports a phase diagram in the $H_x - H_y$ plane of inelastic curvatures. The equilibrium positions in (a) are labeled according to the control points in (b).

4.2. Multi-parameter actuation: stable transitions

Having two independent control parameters offers novel possibilities to induce the transitions $A_3 \leftrightarrow A_2$ between the two stable equilibria. Assume as before that the plate has an initial inelastic curvature H_A and is in the configuration A_3. A fundamentally new type of transition is obtained by using an actuation path circumventing the cusp point P in the clockwise sense. A simple example is the actuating path $ACDEA$ in Fig. 3(b), composed of four steps:

- (AC) a negative change, say ΔH, of the inelastic curvature in the x direction: the configuration moves from A_3 to C in Fig. 3(a);
- (CD) a positive change ΔH of the inelastic curvature in the y direction: the configuration moves from C to D in Fig. 3(a):

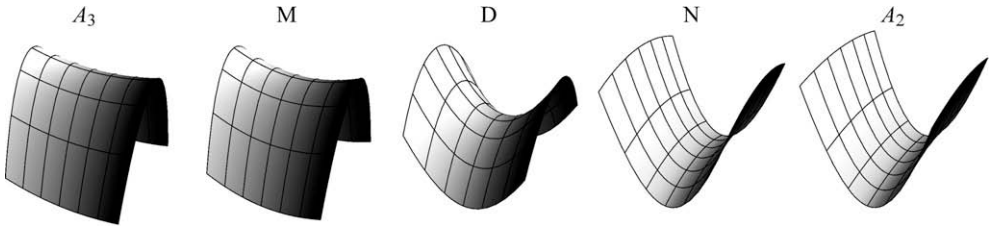

Fig. 4. Stable equilibrium configurations of the plate along the stable transition path from A_3 to A_2. The shapes correspond to points A_3, M, D, N and A_2 in Fig. 3(a).

- (DE) a positive change ΔH of the inelastic curvature in the x direction: the configuration moves from D to E in Fig. 3(a);
- (EA) a negative change ΔH of the inelastic curvature in the x direction, which restore the initial inelastic curvature H_A: the configuration moves from E to A_2 in Fig. 3(a).

The final result is the same as the one obtained with the single-parameter actuation: the passage $A_3 \rightarrow A_2$, the plate being able to hold the two configurations without a persistent actuation. But the transition is obtained with a fundamentally different process: *the configuration A_2 is reached in a purely quasi-static way, without any kind of instability and dynamic phenomenon*. Indeed, the system configuration remains always within the stability region of Fig. 3(a). Fig. 4 shows the shapes of the plate during the transition (see also the Supplementary Material S2). Remarkably, the shape-change takes place almost exclusively around the point D close to the cusp point P, where the sensitivity of the equilibrium curvatures on the control parameters H is very high. The proposed path, being suggested by the global multiparametric stability analysis of the previous Section, is counter-intuitive on the basis of a local sensitivity analysis: to move from a configuration with a large K_y (A_3) to a configuration with a large K_x (A_2), it starts decreasing the inelastic curvature H_x. Note that the reverse passage $A_2 \rightarrow A_3$ is obtained with the counter-clockwise actuating path ($AEDCA$).

5. Applicative example and finite element validation

We illustrate the two-parameter actuation technique proposed in Section 4.2 by revisiting the example of the piezoelectric actuation of a class of bistable unsymmetric cross-plies studied by Schultz et al. (2006), Bowen et al. (2007), and Portela et al. (2008). To this end, consider a square laminate plate of side $L = 0.25$ m with the $[0^\circ_{\text{MFC}}/90^\circ_{\text{AS4}}/0^\circ_{\text{AS4}}/90^\circ_{\text{MFC}}]$ stacking sequence of Fig. 5(a). The central AS4 layers of thickness $h_1 = 0.36$ mm are elastics, the outer layers are commercially available piezoelectric Macro-Fiber Composites[3] of thickness $h_2 = 0.3$ mm produced by Smart-Material, Inc. We suppose that the piezoelectric layers cover the whole plate. Given the material properties of the commercially available materials (see Table 1), we perform numerical experiments on a plate whose geometry and stacking sequence is designed with two objectives: (i) to obtain at ambient temperature a bistable system thanks to the thermal strains associated to the curing process; (ii) to get a piezoelectric effect strong enough to control the shape of the structure. The actuating parameters are the voltages V_0 and V_{90} applied to the upper and lower piezoelectric layers. According to a simplified model, the voltages induce uniaxial membrane strains in each MFC layer, through the constants β_1 of Table 1. Once homogenized over the thickness, they control piezoelectrically induced inelastic curvatures and membrane deformations of the whole plate. As shown by our model, the membrane deformations do not have any relevant effect for the case of a free plate.

Finite element numerical simulations with shell elements are performed exploiting the commercial code Abaqus. Abaqus includes composite shell elements with thermally induced membrane and bending deformations, but not piezoelectric shell elements (Abaqus Inc., 2007). Hence, the piezoelectric effect is modeled by assigning to the MFC layers an equivalent thermal expansion coefficient according to the β_1 constant. The four-layer laminate is assembled by bonding together three composite shells: the top and bottom MFC layers and the $[90^\circ_{\text{AS4}}/0^\circ_{\text{AS4}}]$ elastic cross-ply. Each shell is modeled using the standard Abaqus laminate model. This assembly allows us to introduce layerwise inelastic strain through three independent parameters: one associated to the temperature T of the central elastic cross-ply, the other two to the voltages V_0 and V_{90} of the top and bottom piezoelectric layers. The bonding constraint between the central elastic shell and the outer MFC layers is imposed through the specific Abaqus command *TIE. A similar modeling technique is adopted in Portela et al. (2008).

In common manufacturing process, the two AS4 layers are assembled at high temperature, while the piezoelectric layers are bonded after curing, at ambient temperature. An accurate numer-

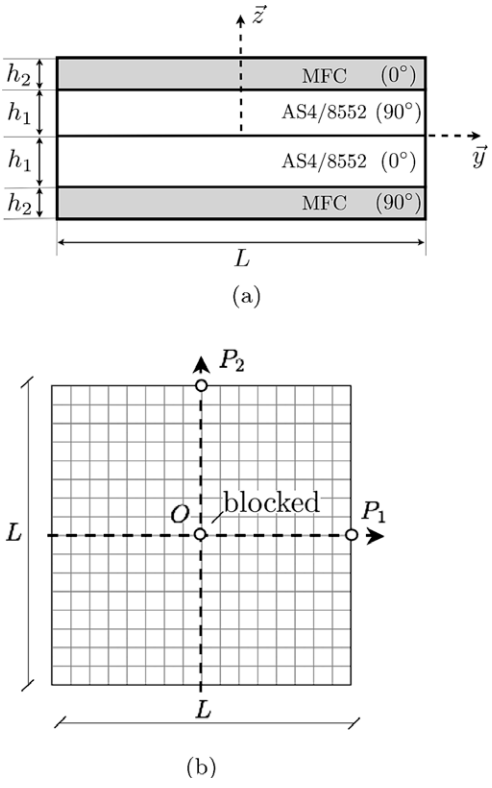

Fig. 5. Square composite plate used for the finite element simulations: (a) layup; (b) top view with finite element mesh (displacements and rotations at the center O are blocked).

[3] The MFC layer is made of piezoelectric fibers embedded in an epoxy matrix and is actuated using interdigitated electrodes.

Table 1
Material properties for the AS4 and MFC layers used in the numerical case study.

	E_1 (GPa)	E_2 (GPa)	G_{12} (GPa)	ν_{12}	α_1 (10^{-6}/°C)	α_2 (10^{-6}/°C)	β_1 (10^{-6}/V)
AS4/8552	135.	9.5	5.0	0.3	−0.02	30.0	–
MFC	30.34	15.86	5.52	0.31	–	–	0.75

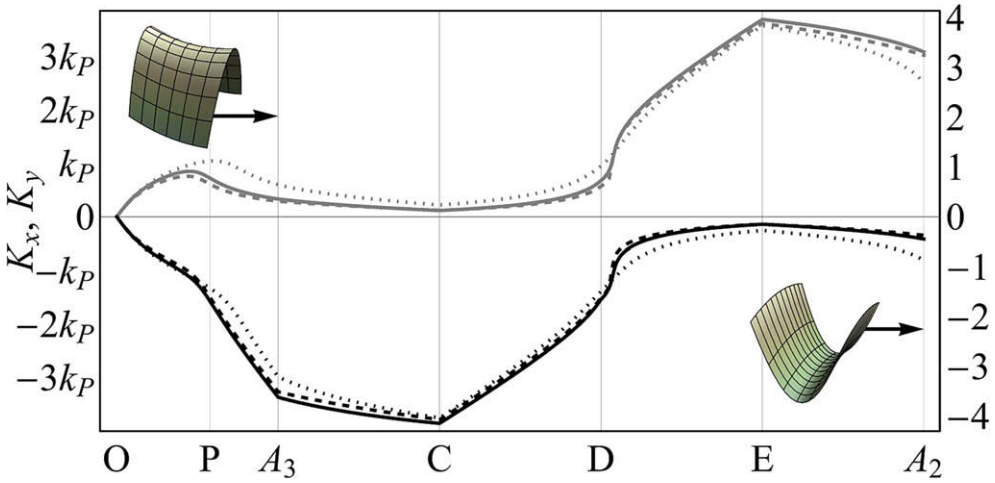

Fig. 6. Comparison of average curvatures K_x (gray) and K_y (black) along the path OACDEA in Fig. 3. Solid lines: finite element model; dashed lines: uniform curvature model with $R_0 = 4.5$ m; dotted lines: uniform curvature model with $R_0 = 3.27$ m. The ticks on the y-axis report both the non-dimensional (left, scaled with $R_0 = 4.5$ m) and dimensional curvatures (right, in meters).

ical simulation of a similar assembling procedures requires to elaborate a careful numerical model (see Portela et al., 2008 for a detailed discussion of the related issues). For sake of simplicity, in our numerical work the elastic plate and the piezoelectric actuators are bonded together in a flat unstressed configuration before applying to the elastic cross-ply the temperature loading of the curing process. This procedure would imply some discrepancies of the simulations presented hereafter from a real physical system. However, it will fit our main goal, which is to illustrate by a simple example the two-parameter actuating concept and to validate the results of the simplified analytical model.

Each of the three shells composing the plate is meshed with identical uniform structured mesh made of 16×16 rectangular general shell elements with eight-nodes and reduced integration (Abaqus S8R elements). The numerical simulation are performed using the Abaqus quasi-static procedure (*STATIC) including geometrical non-linearities (*NLGEOM) through a Full Newton scheme without any stability control or fictitious viscoelastic effects.

To reproduce the multi-parametric actuation path proposed in Section 4.2, we apply the following five loading steps, named accordingly to the corresponding inelastic curvatures in Fig. 3(b): (OA) curing process with the application of a through-the-thickness uniform temperature loading $T = -200$ °C to the central elastic cross-ply[4]; (AC) actuation at the top piezoelectric layer with $V_0 = 580$ V; (CD) actuation at the bottom piezoelectric layer with $V_{90} = 580$ V; (DE) realising the actuation of the top piezoelectric layer by re-setting $V_0 = 0$ V; (EA) realising the actuation of the bottom piezoelectric layer by re-setting $V_{90} = 0$ V.

At the end of the temperature loading *OA* the plate is bistable. In order to converge with the finite element model to a specific stable shape using a square plate, we introduced a small imperfection modifying the thermal expansion coefficient of the top layer (90°) of the central elastic cross-ply to $\alpha_2 = 29.0 \times 10^{-6}\,°C^{-1}$. Coherently, at the end of the step *OA* the plate assumes a quasi-cylindrical shape of the type A_3 in Fig. 3(a), with a large curvature in the y direction.

Fig. 6 reports the curvatures K_x and K_y obtained when varying the inelastic curvatures along the loading path *OACDEA*. The finite element results are compared to the outcomes of the analytical two-degree-of-freedom uniform curvature model. In the uniform curvature model the matrices A, B, and D of Eq. (3) and the non-dimensional bending stiffness of Eq. (4) are calculated using the standard formulas of the laminate theory (see e.g. Berthelot, 1999). For the finite element model (continuous line in Fig. 6), we report the average of the curvatures, estimated from the transverse displacements of the points P_1 and P_2 of Fig. 5(b) through the formulas: $k_x = 8w(P_1)/L^2$, $k_y = 8w(P_2)/L^2$. Comparing the non-dimensional curvatures of the analytical model to the dimensional curvatures of the finite element model requires to assign the value of the scaling radius of curvature R_0. Solving numerically the membrane problem of Section 2.5 with the method suggested in Remark 2.1, we find $R_0 = 3.27$ m. With this scaling radius the analytical model gives the dotted curves of Fig. 6, which are in a reasonable, but not excellent, agreement with the numerical results. The scaling radius giving the best fit between analytical and numerical results is $R_0 = 4.5$ m, corresponding to the dashed curves of Fig. 6. This discrepancy is probably related to the non-uniformity of the actual curvature field. Fig. 7 shows the curvature fields at the equilibrium positions $A_{2,3}$ as obtained with the finite element model, showing the boundary effects neglected in the uniform curvature model.

The results of Fig. 6 provide a nice validation of the simplistic uniform curvature model. Especially, the finite element results confirm that the proposed two-parameter actuating path is suitable to control the passage between the two stable equilibrium positions $A_{2,3}$ avoiding any type of instability. Indeed, the finite ele-

[4] This loading corresponds to the cooling down from a high temperature, say 225 °C, to the ambient temperature, say 25 °C.

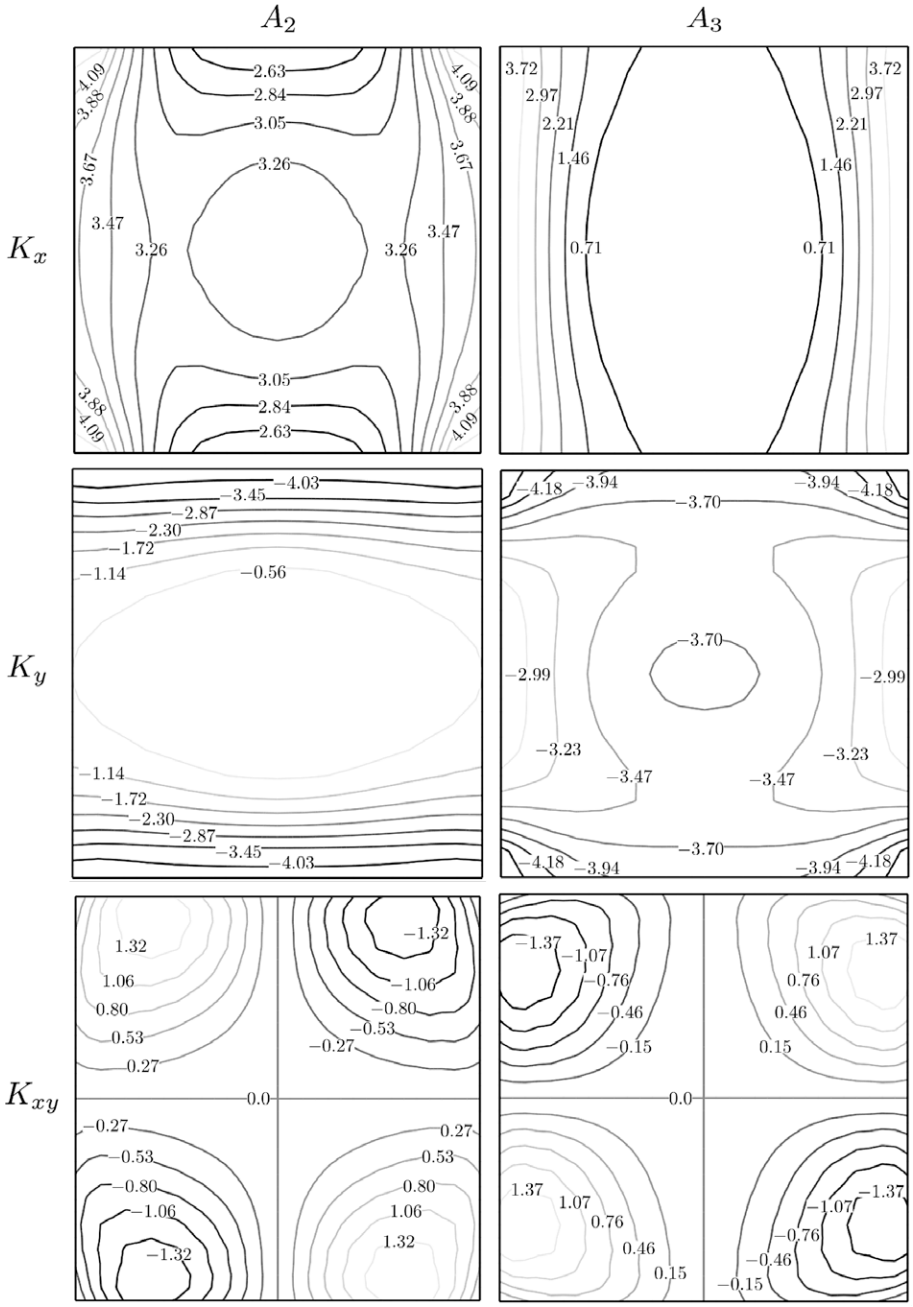

Fig. 7. Curvature fields resulting from finite element simulations: contourplots of the K_x, K_y and K_{xy} at the A_2 (left column) and A_3 (right column) configurations. Dimensional curvature are obtained multiplying the scaling curvature $1/R_0 = 1/4.5$ m.

ment procedure is based on an incremental Newton algorithm, which would not converge if any eigenvalue of the tangential stiffness matrix is negative.

6. Concluding remarks

This paper has analyzed the effect of inelastic deformations and a multi-parametric embedded actuation on bistable orthotropic plates free at the boundaries. Starting with a Föppl–Von Kármán model and assuming the curvature field as constant throughout plate, a three-degree of freedom model in terms of the components of the average curvature tensor has been deduced. Uniform inelastic curvatures in the two coordinate directions have been regarded as free loading parameters; they may account for a wide range of effects including thermal loads or the presence of piezoelectric active layers. With this simplified model, we have been able to produce closed-form solutions relating the stability properties of the plate (positions and number of stable equilibria, bistability regions, stability boundaries) to the applied inelastic curvatures. In this respect, we generalized to orthotropic plates some literature results for isotropic plates. Moreover, a global two-parameter stability analysis has allowed us to get a further insight on the results available for one-parameter loadings. This has suggested alternative actuation paths for controlling a continuous and reversible transition between the stable equilibria. We have shown that with a suitable multi-parameter actuation it is possible to get the transition avoiding snap-through instabilities. This actuating mode has been successfully validated by finite element simulations performed with a commercial code. The numerical work has been concerned

with the applicative case study of a bistable cross-ply laminate with thermal loads and two-parameter piezoelectric actuation. We believe that the numerical results, obtained with realistic geometric and material parameters, furnish a first positive indication of the technological feasibility of the proposed approach. Nevertheless, additional work will be required for the actual experimental implementation and prototyping. This will include design optimization, imperfection sensitivity analysis, and accounting for more complex physical effects, as hygroscopic loads and plastic effects, or specific manufacturing conditions. An important point to be investigated is the influence of boundary conditions and the effect of the integration of the proposed bistable device in more complex structural members (see e.g. Mattioni et al., 2009).

Appendix A. Supplementary data

Supplementary data associated with this article can be found, in the online version, at doi:10.1016/j.ijsolstr.2010.02.007.

References

Abaqus Inc., 2007. Analysis User's Manual, Version 6.7. Dassault Systèmes.

Berthelot, J., 1999. Materials. Mechanical Behavior and Structural Analysis. Springer, New York.

Bowen, C., Butler, R., Jervis, R., Kim, H., Salo, A., 2007. Morphing and shape control using unsymmetrical composites. Journal of Intelligent Material Systems and Structures 18, 89–98.

Ciarlet, P., Gratie, L., Mardare, C., 2009. Intrinsic methods in elasticity: a mathematical survey. Discrete and Continuous Dynamical Systems 23, 133–164.

Dano, M., Hyer, M., 2002. Snap-through behavior of unsymmetric fiber-reinforced composite laminates. International Journal of Solids and Structures 39, 175–198.

Dervaux, J., Ben Amar, M., 2008. Morphogenesis of growing soft tissues. Physical Review Letters 101 (6), 068101.

DiCarlo, A., Quiligotti, S., 2002. Growth and balance. Mechanics Research Communications 29, 449–456.

Dunn, M., Zhang, Y., Bright, V., 2002. Deformation and structural stability of layered plate microstructures subjected to thermal loading. Journal of Microelectromechanical Systems 11 (4), 372–384.

Finot, M., Suresh, S., 1996. Small and large deformation of thick and thin-film multilayers: effects of layer geometry, plasticity and compositional gradients. Journal of the Mechanics and Physics of Solids 44 (5), 683–721.

Forterre, Y., Skotheim, J.M., Dumais, J., Mahadevan, L., 2005. How the venus flytrap snaps. Nature 433, 421–425.

Freund, L., 2000. Substrate curvature due to thin film mismatch strain in the nonlinear deformation range. Journal of the Mechanics and Physics of Solids 48, 1159–1174.

Gigliotti, M., Wisnom, M., Potter, K., 2004. Loss of bifurcation and multiple shapes of thin [0/90] unsymmetric composite plates subject to thermal stress. Composite Science and Technology 64, 109–128.

Guest, S., Pellegrino, S., 2006. Analytical models for bistable cylindrical shells. Proceedings of the Royal Society A: Mathematical, Physical and Engineering Sciences 462, 839–854.

Hyer, M., 1981a. Calculations of the room-temperature shapes of unsymmetric laminates. Journal of Composite Materials 15, 296–310.

Hyer, M., 1981b. Some observations on the cured shape of thin unsymmetric laminates. Journal of Composite Materials 15, 175–194.

Love, A., 1906. A Treatise on the Mathematical Theory of Elasticity. Cambridge University Press, Cambridge, UK.

Mansfield, E., 1989. The Bending and Stretching of Plates. Cambridge University Press, Cambridge, UK.

Mattioni, F., Weaver, P., Potter, K., Friswell, M., 2007. Analysis of thermally induced multistable composites. International Journal of Solids and Structures 45, 657–675.

Mattioni, F., Weaver, P.M., Friswell, M.I., 2009. Multistable composite plates with piecewise variation of lay-up in the planform. International Journal of Solids and Structures 46 (1), 151–164.

Maurini, C., Pouget, J., Vidoli, S., 2007. Distributed piezoelectric actuation of a bistable buckled beam. European Journal of Mechanics A/Solids 26, 837–853.

Norman, A.D., Seffen, K., Guest, S., 2008. Multistable corrugated shells. Proceedings of the Royal Society A: Mathematical, Physical and Engineering Sciences 464, 1653–1672.

Norman, A.D., Seffen, K., Guest, S., 2009. Morphing of curved corrugated shells. International Journal of Solids and Structures 46, 1624–1633.

Portela, P., Camanho, P., Weaver, P., Bond, I., 2008. Analysis of morphing, multistable structures actuated by piezoelectric patches. Computers and Structures 86, 347–356.

Potter, K., Weaver, P., Abu Seman, A., Shah, S., 2007. Phenomena in the bifurcation of unsymmetric composite plates. Composites. Part A: Applied Science and Manufacturing 38, 100–106.

Salamon, N., Master, C., 1995. Bifurcation in isotropic thin film/substrate plates. International Journal of Solids and Structures 32 (3/4), 473–481.

Schultz, M.R., Hyer, M.W., Williams, R., Wilkie, W.K., Inman, D.J., 2006. Snap-through of unsymmetric laminates using piezocomposite actuators. Composites Science and Technology 66, 2442–2448.

Seffen, K., 2007. 'Morphing' bistable orthotropic elliptical shallow shells. Proceedings of the Royal Society A: Mathematical, Physical and Engineering Sciences 463, 67–83.

Seffen, K., McMahon, R., 2007. Heating of a uniform wafer disk. International Journal of Mechanical Sciences 49, 230–238.

Vidoli, S., Maurini, C., 2008. Tristability of thin orthotropic shells with uniform initial curvature. Proceedings of the Royal Society A: Mathematical, Physical and Engineering Sciences 464, 2949–2966.

Zhang, Y., Dunn, M., 2004. Geometric and material nonlinearity during the deformation of micron-scale thin-film bilayers subject to thermal loading. Journal of the Mechanics and Physics of Solids 52, 2101–2126.